HHS Public Access

Author manuscript

*Oncogene*. Author manuscript; available in PMC 2022 April 18.

Published in final edited form as:

*Oncogene*. 2021 December ; 40(50): 6759–6771. doi:10.1038/s41388-021-02040-9.

# Loss of the Wild-type *KRAS* Allele Promotes Pancreatic Cancer Progression through Functional Activation of YAP1

**Han Yan**[1,2,†], **Chih-Chieh Yu**[1,2,†], **Stuart A. Fine**[2], **Ayman Lee Youssof**[2], **Ye-Ran Yang**[1], **Jun Yan**[3], **Dillon C. Karg**[2], **Edwin C. Cheung**[2], **Richard A. Friedman**[2,4], **Haoqiang Ying**[5], **Emily I. Chen**[2,6], **Ji Luo**[7], **Yi Miao**[8], **Wanglong Qiu**[1,2], **Gloria H. Su**[1,2,9,10,*]

[1]The Department of Pathology & Cell Biology, Columbia University Irving Medical Center, New York, NY 10032

[2]Herbert Irving Comprehensive Cancer Center, Columbia University Irving Medical Center, New York, NY 10032

[3]Department of Pathology, Tianjin First Center Hospital, Tianjin, TJ 300192, China

[4]Biomedical Informatics Shared Resource, Herbert Irving Comprehensive Cancer Center, and Department of Biomedical Informatics, Columbia University Irving Medical Center, New York, NY 10032

[5]Molecular and Cellular Oncology Department, The University of Texas MD Anderson Cancer Center, Houston, Texas

[6]Department of Pharmacology, Columbia University Irving Medical Center, New York, NY 10032

[7]Laboratory of Cancer Biology and Genetics, Center for Cancer Research, National Cancer Institute, Bethesda, MD 20892

[8]Pancreas Center & Department of General Surgery, The First Affiliated Hospital of Nanjing Medical University, Nanjing 210029, Jiangsu, China

[9]Department of Otolaryngology and Head & Neck Surgery, Columbia University Irving Medical Center, New York, NY 10032

[10]Pancreas Center, Columbia University Irving Medical Center, New York, NY 10032



[*]To whom correspondence should be addressed: Gloria Su, 1130 St. Nicholas Ave, ICRC 10-04, New York, NY 10032, gs2157@columbia.edu.

Authors' contribution

HY and CY were responsible for the designs of the experiments, the acquisition, analyses, interpretation, and presentation of the data, and drafting the manuscript. SAF, ALY, YY, JY, DCK, ECC, EIC, and WQ contributed to the acquisition and analyses of the data. RAF, HY (Ying), and EIC were responsible for the computational analyses, statistical analyses, and interpretation of the data. EIC, JL, YM, and GHS provided resources and materials that were vital to the completion of the work. HY, CY, SAF, RAF, EIC, JL, WQ, and GHS prepared and revised the manuscript. WQ and GHS conceived and designed the work that led to the submission. Each author has made substantial contributions to the work and/or have been involved in drafting or revising the manuscript. All the authors have given final approval of the version to be published and take public responsibility for appropriate portions of the content.

[†]Both of these authors contributed equally to this work. The current affiliation for HY is the Pancreas Center & Department of General Surgery, The First Affiliated Hospital of Nanjing Medical University, Nanjing 210029, Jiangsu, China

Competing Interests

Other than the grants listed in the acknowledgement section, the authors declare that they have no other competing interests.

## Abstract

Human pancreatic ductal adenocarcinoma (PDAC) harboring one KRAS mutant allele often displays increasing genomic loss of the remaining wild-type (WT) allele (known as LOH at *KRAS*) as tumors progress to metastasis, yet the molecular ramification of this WT allelic loss is unknown. In this study, we showed that the restoration of WT KRAS expression in human PDAC cell lines with LOH at *KRAS* significantly attenuated the malignancy of PDAC cells both *in vitro* and *in vivo*, demonstrating a tumor suppressive role of the WT *KRAS* allele. Through RNA-Seq, we identified the HIPPO signaling pathway to be positively regulated by WT KRAS in PDAC cells. In accordance with this observation, PDAC cells with LOH at *KRAS* exhibited increased nuclear localization and activation of transcriptional coactivator YAP1. Mechanistically, we discovered that WT KRAS expression sequestered YAP1 from the nucleus, through enhanced 14-3-3zeta interaction with phosphorylated YAP1 at S127. Consistently, expression of a constitutively-active YAP1 mutant in PDAC cells bypassed the growth inhibitory effects of WT KRAS. In patient samples, we found that the YAP1-activation genes were significantly upregulated in tumors with LOH at *KRAS*, and YAP1 nuclear localization predicted poor survival for PDAC patients. Collectively, our results reveal that the WT allelic loss leads to functional activation of YAP1 and enhanced tumor malignancy, which explains the selection advantage of the tumor cells with LOH at *KRAS* during pancreatic cancer clonal evolution and progression to metastasis, and should be taken into consideration in future therapeutic strategies targeting KRAS.

## Introduction

Pancreatic ductal adenoma carcinoma (PDAC) is the third leading cause of cancer deaths in the United States. Despite the increased understanding of its molecular events, most of those patients will die from pancreatic cancer within 5 years [1]. The therapeutic efficacy of the current first-line chemotherapeutic drugs, gemcitabine plus Abraxane or FOLFIRINOX, has shown clinical benefit and slightly improved survival over gemcitabine alone, but still remain unsatisfactory [2]. Therefore, new therapeutic targets and approaches are urgently needed for the vast majority of pancreatic cancer patients. As the result, there has been a renewed interest in targeting the once thought to be undruggable KRAS [3, 4].

Activation of the *KRAS* oncogene, usually by point mutations in codon 12, is observed in ~95% of PDAC patients. KRAS is a member of the Ras family of small GTPases that regulates cell growth, differentiation, and survival through the activation of key downstream pathways, including MAPK and PI3K/AKT signaling [5]. In addition to activating point mutations, an imbalance between the wild-type (WT) allele and the mutant allele of *KRAS* has been associated with poor prognosis in cancer patients. This phenomenon, termed “mutant allele-specific imbalance” (MASI), reflects higher dosage of the mutant allele over its WT counterpart [6, 7]. MASI has been identified in various cancers harboring *KRAS* mutations, such as pancreatic, lung, and colorectal cancers [7-11]. While the underlying molecular mechanism remains elusive, it has been proposed that tumorigenesis is influenced by the relative expression levels or the copy number ratio of the WT and mutant KRAS alleles [9, 10, 12]. The dominance of the mutant allele over the wild-type allele may result from selective amplification of the mutant allele (partial MASI or MASI with copy number

gain, Fig. S1) [10], as *KRAS* mutations have been associated with higher *KRAS* gene copy number [12, 13], however, less appreciated is the fact that MASI can also result from loss of the WT allele (or commonly described as loss of heterozygosity, LOH), which leads to complete MASI (Fig. S1) [7, 10, 12].

Loss of the WT allele or LOH at the RAS loci has been reported in both murine and human tumors [7, 8, 12, 14], yet the significance of this allelic loss has long been debated. Genetic studies have shown that WT KRAS can function as a tumor suppressor in the context of oncogenic KRAS [15-19], implying that LOH at *KRAS* may offer growth advantage to cancer cells. Indeed, in our genetically-engineered mouse model (GEMM) for PDAC, we detected increased incidence of LOH at *Kras* as PDAC progressed to metastasis [8]. Comparing human PDAC cell lines derived from the primary *vs*. metastasis sites, we discovered that LOH at chromosome 12p, where *KRAS* resides, is the singular chromosomal loss associated with metastasis [8]. Given that pancreatic cancer is believed to be driven by epigenomic reprogramming rather than a genomic mutation signature [20, 21], the fact that LOH at chromosome 12p is the only significant genomic alternation known to be associated with pancreatic cancer metastasis is notable. In a subsequent study, we demonstrated that increased loss of WT *KRAS* allele is also associated with lung cancer metastasis in humans [7]. Our data is further supported by a recent report that LOH at *KRAS* is a frequent event (>30%) in human and murine PDAC[12]. Taken together, these data suggest that loss of the WT *KRAS* allele (complete MASI) must offer tumor cells growth advantage in clonal evolution, hence an increased frequency of LOH at *KRAS* is detected among metastases. Given the growing evidence that genomic loss of the WT *KRAS* allele is advantageous in tumor progression and metastasis, in this study we aimed to identify genes and pathways that are perturbed by this allelic loss using unbiased RNA-Seq and proteomic approaches, in hope to dissect the tumor-suppressive role of WT KRAS from the oncogenic function of mutant KRAS to improve future target therapies in oncogenic KRAS-driven cancers.

## Results

### Wild-type (WT) KRAS suppressed tumor malignancy

To investigate the functional and molecular ramifications of the WT *KRAS* allelic loss in the context of oncogenic *KRAS* (LOH at *KRAS*), we restored WT KRAS expression in two PDAC cell lines which had spontaneously lost the WT *KRAS* allele (both with complete MASI, Fig. S1). The MIA PaCa-2 line, which harbors a G12C mutation in *KRAS*, has lost its WT *KRAS* allele with amplification of the mutant *KRAS* allele. AsPC-1 harbors a G12D mutation and has lost its WT *KRAS* allele without amplification of the mutant allele [7, 8]. The stably transduced cell lines, iWT-KRAS-MIAPaCa-2 and iWT-KRAS-AsPC-1, expressed the WT *KRAS* mRNA and protein upon doxycycline (Dox) induction in a dosage- and time-dependent manner (Fig. 1A, B). We observed a statistically significant reduction in cell growth, colony formation, and cell motility resulted from WT KRAS restoration in iWT-KRAS-MIA PaCa-2 (Fig. 1C-G). Comparable results were observed in multiple iWT-KRAS-Mia PaCa-2 and iWT-KRAS-AsPC-1 clones (Fig. S2), demonstrating that the tumor-suppressive effects induced by the restoration of WT KRAS were independent of cell lines, clonal effects, and/or *KRAS* mutation subtype. The Dox treatment did not affect the

RNA expression level of the endogenous mutant *KRAS* (Fig. S3A) nor evoke unspecific toxicity in these cancer cells (Fig. S3B-E). To investigate whether WT KRAS-induced tumor suppressive effects were mediated by the altered ratio of the WT *KRAS* allele to the mutant allele or by the mere presence of the wild-type allele, we generated iWT-KRAS-PANC-1 cells, which harbor heterozygous G12D mutation with copy number gain (partial MASI, Fig. S1). The expression of exogeneous WT KRAS did not elicit significant functional changes in iWT-KRAS-PANC-1 cells (Fig. S4). This differential impacts of the WT *KRAS* allele on the complete MASI cell lines (MIA PaCa-2 and AsPC-1) *vs*. partial MASI cell line (PANC-1) suggest that the mere presence of the WT *KRAS* allele plays a larger role than the dosage of the total KRAS protein or the ratio of WT to mutant *KRAS* alleles in the WT KRAS-mediated tumor suppression.

The effects of the WT KRAS expression on tumorigenicity were then further investigated *in vivo* by subcutaneous implantations of iWT-KRAS-MIA PaCa-2 cells or MIA PaCa-2 control in nude mice. We observed that the restoration of WT KRAS significantly reduced tumor volumes in the xenografted nude mice (Fig. 1H-I, S5). Collectively, these results demonstrate that the expression of WT *KRAS* in pancreatic cancer cells that had spontaneously lost the WT *KRAS* allele would attenuate tumor malignancy both *in vitro* and *in vivo*.

## WT KRAS attenuated YAP1 nuclear localization and activities

To delineate the underlying mechanisms responsible for the tumor inhibitory effects of WT KRAS, RNA-Seq analysis was performed to identify genes and pathways perturbed by the restoration of WT KRAS. Among the differentially expressed genes, profoundly, genes associated with active HIPPO signaling pathway were significantly represented upon WT KRAS restoration (Fig. 2A). Yes-associated protein 1 (YAP1) is a major transcriptional co-activator that regulates organ size, proliferation and tumor growth, and is normally controlled by the HIPPO pathway [22, 23]. However, when deregulated, YAP1 acts as a potent oncogene that can promote tumorigenesis in a wide range of tissues. Further analysis of our RNA-Seq data revealed that "YAP1 activation signature" (genes that are known to be associated with YAP1 activation [24]) were differentially downregulated in Dox-treated iWT KRAS MIA PaCa-2 cells compared to vehicle-treated control (Fig. 2B). Notably, YAP-TEAD target genes, *GADD45A*, *BCAT1*, *TNFRSF12A*, and *CYR61*, were among those negatively regulated by WT KRAS expression.

The results from the RNA-Seq analyses were further tested by ensuing functional studies. Upon doxycycline-induced restoration of WT KRAS expression, a marked retention of YAP1 in the cytoplasm was observed in both iWT-KRAS-MIA PaCa-2 and iWT-KRAS-AsPC-1 cells by immunofluorescence staining (Fig. 2C) and western blot analysis of nuclear *vs*. cytoplasmic fractions (Fig. 2D). Doxycycline treatment did not affect the subcellular distribution of YAP1 in either of the parental cell lines (Fig. 2E), ruling out the potential pitfall that it was a Dox-induced caveat. The observed cytoplasmic retention of YAP1 induced by WT KRAS was further confirmed by semi-quantitative immunocytochemistry (Fig. 2F-G).

Since YAP1 is a transcription coactivator, the effects of WT KRAS expression on YAP1-TEADs transcriptional activities were then measured quantitatively using YAP1-TEADs transcriptional luciferase reporters, HOP-flash (HIP-flash served as the mutated negative control) [25]. As shown in Fig. 3A-B, the endogenous YAP1-TEADs activities were high in both iWT-KRAS-MIA PaCa-2 and iWT-KRAS-AsPC-1 cells, which were drastically attenuated upon the restoration of WT KRAS expression in both cell lines, indicating that WT KRAS not only inhibited YAP1 nuclear translocation but also its transcriptional activities. Consistently, expressions of established YAP1-TEADs target genes were reduced when measured by quantitative PCR (Fig. 3C) [24]. For instance, the RNA expressions of *BMP4* and *CTGF* were among those significantly downregulated by WT KRAS expression.

Proteomic analysis was also conducted comparing cytoplasmic *vs.* nuclear protein expression profiles of Dox-treated *vs.* vehicle-treated iWT-KRAS-MIA PaCa-2 cells at 48-hour time point (Fig. S6). The nuclear expression of the YAP1 protein was significantly reduced in the Dox-treated cells compared to the vehicle-treated control (ANOVA test, $p < 0.01$), consistent with the above finding of YAP1 cytoplasmic retention resulted from the expression of WT KRAS. Of note, the TAZ protein, which is a closely related to YAP1, was unaffected by the WT KRAS expression.

We also examined the two major canonical RAS signaling pathways and found that WT KRAS restoration in the iWT-KRAS-MIA PaCa-2 and iWT-KRAS-AsPC-1 cells did not result in statistically significant attenuation of the MAPK and AKT signaling pathways that could consistently account for the observed WT KRAS-mediated tumor suppression (Fig. S7).

## Constitutively-active YAP1 (S127A) mutant bypassed WT KRAS-induced tumor suppression

YAP1 is negatively regulated in part via phosphorylation at serine 127, which results in 14-3-3zeta binding, YAP1 cytoplasmic retention, and inhibition of YAP1 activity [26]. Accordingly, phospho-YAP1 (S127) levels were upregulated with increasing WT KRAS expression over the time course of Dox treatment in both iWT-KRAS-MIA PaCa-2 and iWT-KRAS-AsPC-1 cell lines (Fig. 3D-E). Co-immunoprecipitation (Co-IP) was performed using anti-14-3-3 pan antibody to pull down proteins bound to 14-3-3, we observed an enhanced interaction of p-YAP1 (S127) and 14-3-3 with the restored expression of WT KRAS (Fig. 3F). These results suggest that cytoplasmic sequestration of YAP1 by WT KRAS may be mediated by enhanced association phospho-YAP1 and 14-3-3zeta, resulting in decreased YAP1 nuclear translocation (Fig. 2C-G), and attenuated transcription of the YAP1-TEADs downstream target genes (Fig. 3A-C).

To further validate that the effects of WT KRAS restoration are dependent on S127 phosphorylation, a plasmid encoding the constitutively active YAP1-S127A mutant [26] was transiently transfected into iWT-KRAS-MIA PaCa-2 cells. Transfections with the vector alone or the WT YAP1 plasmid served as the negative and positive controls, respectively. Western blot analyses showed that the introduction of exogenous YAP1, in either the WT or the mutant form, resulted in increased levels of cytoplasmic YAP1 (Fig. 4A). However, substantially more YAP1 proteins were detected in the nuclear fraction of

the cells transfected with the S127A mutant YAP1 vector irrespective of Dox treatment status, indicating that the defective phosphorylation at S127 enabled YAP1 to bypass the WT KRAS-induced cytoplasmic retention (Fig. 4A). Moreover, in the scratch (Fig. 4B-C) and MTT (Fig. 4D) assays, only YAP1-S127A expressing cells were able to reverse the tumor-suppressive effects of WT KRAS. In contrast, the overexpression of WT YAP1 was not sufficient to rescue cells from the WT KRAS-induced tumor suppression (Fig. 4B-D), thus confirming that regulation of YAP1 phosphorylation at S127 is crucial for WT KRAS-induced tumor suppression (Fig. 4E).

Differentially expressed genes from the RNA-Seq analyses were also compared to the Biological Process branch of the Gene Ontology database, the Gene Ontology categories of 'negative regulation of cell proliferation', 'negative regulation of cell growth', and 'negative regulation of cell migration' were overrepresented in WT KRAS restored *vs.* control with *p*-values of 0.000024, 0.00027, and 0.00034, respectively. These molecular signatures are consistent to and supportive of the functional tumor-suppressive phenotypes associated with WT KRAS restoration.

## Activated YAP1 predicted poor prognosis in PDAC patients

To assess the clinical significance of YAP1 activation in PDAC patients, we examined YAP1 nuclear expression in PDAC tissue microarrays (TMAs, n=92) by immunohistochemistry (IHC). We only considered nuclear labeling of YAP1 to be positive, given that YAP1 functions as a transcriptional activator. Quantification of YAP1 was analyzed by an H-score that takes into account both the percentage and intensity of cell staining [27]. IHC results were divided into three groups according to their final H-score value: Negative (n=32, H-score ≤ 0.1), Low (n=27, 0.1<H-score ≤ 0.6), and High (n=33, 0.6<H-score) (Table S1, Fig. 5A). High YAP1 nuclear expression was associated with poorer prognosis in the Kaplan-Meier survival analysis compared to the Negative group and the Negative/Low groups combined ($p < 0.05$, Mantel-Cox test) (Fig. 5B). Furthermore, median survival days decreased with higher nuclear YAP1 expression (Fig. 5C), confirming that YAP1 nuclear expression was reversely correlated with long-term survival rates in PDAC patients.

YAP1 activation signature (genes that are known to be associated with YAP1 activation) is recently reported to be enriched in the squamous/basal subtype of human PDAC [28], which has the worst prognosis among all PDAC subtypes [29]. Using the same YAP1 activation signature [24] and human PDAC from TCGA collection by Tu *et al*, [28], we investigated if LOH at the *KRAS* locus is associated with PDAC subtypes and/or the YAP1 activation signature. We detected LOH at the *KRAS* locus at high frequency in the squamous/basal (3/7 or 42.9%, red) and progenitor/classical subtypes (10/32 or 31.3%, cyan), but not in the PDAC samples with mix (n=2, yellow) or unknown subtypes (n=8, grey). Although LOH at *KRAS* did not segregate exclusively with the more aggressive squamous/basal subtype in the hierarchical clustering analysis (Fig. S8), however importantly, within each of the squamous/basal or progenitor/classical subtype, YAP1 activation signature clustered with the LOH at *KRAS* status (Fig. S8). Consistent with the hierarchical clustering analysis, elevated expressions of YAP1 activation genes were observed in the cases with LOH at *KRAS* compared to those without LOH within each subtype (Fig. 5D). Moreover, we detected

statistically significant elevated expressions of the YAP1 activation genes in PDAC with LOH at *KRAS* as a group without subtypes differentiation (Fig. 5E), providing evidence that LOH at *KRAS* led to functional YAP1 activation in human PDAC.

## Discussion

RAS, the founder member of the family of GTPases, serves as a regulator of cellular signaling. Alternating between the GDP-bound and GTP-bound form, it regulates diverse phenotypes such as proliferation, differentiation, senescence, and apoptosis [5]. In recent years, there have been considerable debates over whether WT RAS plays a supporting role for an oncogenic RAS (cognate or another RAS isoform), or WT RAS possess an independent role in tumor suppression [14-18, 30-34]. It is also equally contentious how tumor-suppressive WT KRAS antagonizes mutationally activated KRAS. One possibility is that WT KRAS simply competes with mutant KRAS in the canonical RAS/RAF/MAPK signaling pathway. This is supported by evidence that RAS functions as a homodimer and WT-mutant KRAS dimer is less effective compared to mutant-mutant dimers in activating MAPK signaling pathway [18, 33]. The other possibility is that the tumor-suppressive signaling of WT KRAS is independent from the canonical oncogenic RAS signaling pathway, which is supported by our discovery of the WT KRAS-HIPPO-↓YAP1 signaling axis in this current study.

We and others have reported that loss of the wild-type *KRAS* allele with concomitant mutated *KRAS* (LOH at *KRAS*) is a frequent event (>~30%) [8, 12] and associated with metastasis in pancreatic and lung cancers[7, 8, 12]. Deletion of the WT *KRAS* allele in colorectal cancer cell lines also increased growth in soft agar when compared to their isogenic parental cell lines [35]. In this study we aimed to identify genes and pathways that are perturbed by this allelic loss, in hope to understand the broader implications of this allelic loss, and to dissect the tumor-suppressive role of WT KRAS from the oncogenic function of mutant KRAS in oncogenic KRAS-driven cancers. Leveraging the two human pancreatic cancer lines that we have previously shown to display complete MASI at the *KRAS* locus [7, 8], we observed that the restored expressions of WT KRAS suppressed the growth, invasiveness, and motility of these PDAC cell lines *in vitro* and inhibited tumor growth in *vivo* (Fig. 1, S2, S5). Notably, overexpression of exogenous WT KRAS did not elicit additional tumor-suppressive effects in pancreatic cancer cells with endogenous WT *KR*AS expression (Fig. S4), signifying that it's the presence of the WT allele, more than the dosage, that is more pertinent to its tumor-suppressive functions.

Using the unbiased RNA-Seq approach, we identified genes associated with active HIPPO signaling pathway were significantly represented upon WT KRAS restoration (Fig. 2 and 3). YAP1 is a major transcriptional effector of the functionally conserved Hippo pathway, which is a crucial regulator of organ size, proliferation and tumor growth [22, 23]. YAP1 is reported as a potent oncogene that can promote tumorigenesis in a wide range of tissues [36]. Overexpression of YAP1 in non-transformed cells leads to its nuclear accumulation, resulting in adhesion-independent growth, epithelial to mesenchymal transition (EMT), suppression of apoptosis, and proliferation[22, 23, 37]. Elevated expression of YAP/TAZ have been reported in many cancer types, including PDAC, liver, breast, lung, colon,

ovary, etc [38]. YAP1 activation has been tied to mutant KRAS, either as a downstream mediator or as a mean to bypass KRAS oncogene addiction [39-42]. Overexpression of YAP1 (both cytoplasmic and nuclear YAP1 expressions were scored together in this prior study) has been shown as an independent prognostic marker for overall survival for PDAC patients and associated with liver metastasis [43]. More recently, expression of the YAP1 activation signature was found enriched in the squamous/basal/quasi-mesenchymal subtype of human pancreatic cancer, which is the most aggressive subtype of PDAC [28, 42]. The deletion of YAP1 in GEMM for PDAC significantly reduced their tumor burdens, likely by mitigating pancreatic tumorigenesis at multiple progression points from acinar to ductal metaplasia (ADM), pancreatic intraepithelial neoplasia (PanIN), to invasive PDAC [41, 44]. Collectively, these prior studies have established that YAP1 plays a significant role in PDAC, but focused on the interplays between oncogenic mutant KRAS and YAP1.

In our current study, we revealed a novel mechanism that WT KRAS suppresses tumor progression and metastasis by negative regulation of YAP1. We detected high YAP1 nuclear expression and transcriptional activities in PDAC cells with LOH at *KRAS*, which were markedly reduced upon restoration of WT KRAS expression (Fig. 2 and 3). The negative regulation of YAP1 by WT KRAS is likely mediated via the increased phosphorylation of YAP1 at S127 and enhanced association with 14-3-3 proteins (Fig. 3D-F). Expression of constitutively-activated YAP1-S127A mutant protein rescued pancreatic cancer cells from the growth inhibitory effects of WT KRAS on cell proliferation and motility, confirming the significance of phosphorylation at S127 and that YAP1 is downstream of the WT KRAS tumor-suppressive pathway (Fig. 4). Together, these results offer evidence supporting that genomic loss of the WT *KRAS* allele is not a mere byproduct of genomic instability but rather a selective event that promotes tumor progression to metastasis via YAP1 activation. However, presently it is not apparent to us how WT KRAS expression regulates YAP1 phosphorylation and its cytoplasmic sequestration. Intriguingly, it has been reported previously that mutant KRAS directly binds to tumor suppressor RASSF1A to activate the apoptotic MST2-LATS1 pathway, which leads to subsequent binding of LATS1 to Mdm2, sequestering of Mdm2, and stabilization of p53 and apoptosis in colorectal cancer cells. This mutant KRAS-induced apoptosis is counteracted by WT KRAS, which inhibits the MST2 pathway in part via AKT activation [31, 32]. Although in this scenario in the context of colorectal cancer, WT KRAS plays a prosurvival role, inhibits apoptosis and aids mutant KRAS-mediated cell transformation, yet this previous finding offers a potential mechanistic basis for our future investigations. Numerous members of the RASSF family, such as RASSF2, 4, 5A, 6, and 9, have been observed to interact with KRAS directly [45]. RASSFs is also known to associate with MST1/2 via the SARAH (Salvador-RASSF-Hippo) domain and SAV1 to promote apoptosis [46]. It's conceivable that WT KRAS may either compete with mutant KRAS for association with a RASSF protein, or alternatively, WT KRAS and oncogenic KRAS may interact with different RASSF proteins, which lead to the differential regulations of MST1/2-LATS1/2-YAP1 HIPPO signaling pathway. Given that overexpression of WT KRAS in PANC-1 cells didn't result in inhibition in growth, motility, and invasiveness of the tumor cells (Fig. S4), the latter hypothesis may be more probable. Supporting this potential mechanism, we do detect *RASSF2* (fdr=0.00194), *RASSF1* (fdr=0.00047), *RASSF5* (fdr=0.00068), *RASSF3* (fdr=0.002496), *RASSF4* (fdr=0.004996),

and *RASSF8* (fdr=0.017531) among the differentially expressed genes when comparing the gene expressions with or without Dox-induced WT KRAS expression. Since the RASSF family of protein comprises ten members and eight of them have multiple splice variants [45], comprehensive investigations of which protein(s) may be involved in the WT KRAS-induced YAP1 inactivation would be desirable and necessary in the future. Furthermore, the Gene Ontology categories of 'negative regulation of cell proliferation', 'negative regulation of cell growth', and 'negative regulation of cell migration' were also overrepresented in WT KRAS restored *vs.* control. It would also be of interests to investigate if YAP1 is directly responsible for the differential expressions of the genes in these three categories.

While our Dox-inducible system enabled us to investigate dynamic molecular alterations directly associated with WT KRAS expression, avoiding secondary or tertiary effects associated with cell adaptation that might have occurred after stably knock-in or knock-out a gene of interest. However, one limitation of the current study is that Dox-induced WT KRAS expression might not be at physiological level and was higher than the endogenous mutant proteins in some of the iWT-KRAS-MIAPaCa-2 and iWT-KRAS-AsPC-1 cells examined (Fig. S7A, WT KRAS was 3-folds higher than the oncogenic KRAS in the iWT-KRAS-MIAPaCa-2 cells and 7-folds higher in the iWT-KRAS-AsPC-1 cells at 24-hours timepoint). To mitigate potential caveats, multiple cell lines and clones were employed in our studies. It's also important to note that increased p-YAP1 was observed as early as 8-hours after the Dox-induction (Fig. 3D-E), when WT KRAS was not overexpressed compared to the endogenous mutant KRAS protein (~1:1 or less, Fig. S7A). WT allelic-specific inactivation and/or inducible knock-down of the WT *KRAS* allele in pancreatic cancer cell lines possess both WT and mutant *KRAS* alleles in future studies would be warranted to further verify our findings here.

As alluded to previously, functions of WT KRAS may be complex and context dependent. The expression of WT RAS has been shown to be essential for non-cognate oncogenic RAS-mediated MAPK signaling and cell proliferation [33, 34]. It has also been reported that WT KRAS can counteract apoptosis induced by chronic expression of mutant KRAS and aid mutant KRAS-mediated cell transformation in colorectal cancer cells [31, 32]. Evidence supporting a pure tumor-suppressive role for WT KRAS are equally abundant and perhaps more robust. Using GEMMs, we and others have demonstrated that loss of the WT *KRAS* allele promote tumor progression and increased malignancy in oncogenic KRAS-mediated pancreatic, lung, and T-cell leukemia *in vivo* [8, 12, 15-19]. Ambrogio *et al.* has reported that dimerization of WT KRAS and mutant KRAS triggered a less potent MAPK signaling than dimers of two mutant KRAS proteins and the disruption of WT-Mut KRAS dimers promoted tumor growth, suggesting a mechanism in which WT KRAS mediates tumor-suppression through dimerization [18]. However, in the context of MEK inhibition, WT-Mut KRAS dimerization led to drug resistance and the disruption of this dimerization would render cancer cells more sensitive to MEK inhibitors [18]. In our current study, the Dox-induced WT KRAS expression in iWT-KRAS-MIAPaCa-2 and iWT-KRAS-AsPC-1 cells did not yield pronounced effects on the MAPK and AKT signaling pathways that could account for WT KRAS-mediated tumor suppression consistently (Fig. S7), suggesting a different underlying mechanism from the one proposed by Ambrogio *et al.* Our results agree with our previously reported observations comparing murine pancreatic

tumor cell lines with or without LOH at *Kras* [8]. Similarly, no discernible differences were detected in KRAS-GTP levels, phosphorylation of ERK, phosphorylation of AKT between $KRAS^{Mut/WT}$ *vs.* $KRAS^{Mut/-}$ isogenic colorectal cancer cells under conditions of either basal proliferation in 10% FBS, serum starvation, or acute stimulation with EGF, even though loss of the WT *KRAS* allele consistently increased growth in soft agar [35]. While we did not perceive a consistent perturbation to the MAPK and AKT signaling pathways associated with the expression of WT KRAS across the cell lines examined, we did detect clonal variations (Fig. S7). Since the function of WT KRAS can be context-dependent, future interrogations of these clonal variations may offer new insights to better delineate the differential contexts and how WT KRAS may regulate YAP1 activities.

In supporting of the *in vitro* discoveries, YAP1 nuclear localization was found to be associated with poor prognosis in PDAC patients (Fig. 5A-C). More intriguingly, the genes known to be associated with YAP1 activation were statistical significantly elevated in human PDAC samples with LOH at *KRAS* (Fig. 5E), providing *in vivo* evidence that LOH at *KRAS* led to functional YAP1 activation in human PDAC. In our hierarchical clustering analysis, samples with LOH at *KRAS* clustered together within each subtype with the elevated expression of the YAP1 activation signature (Fig. S8). Consistent with the hierarchical clustering analysis, the expression of the YAP1 activation signature was higher in the cases with LOH at *KRAS* compared to those without LOH within the same subtype (Fig. 5D). Statistical significance was achieved only in the progenitor subtype (n=32), not in the squamous subtype (n=7), which may be due to the small sample size of the squamous subtype in the current study or the already higher YAP1 activation exhibited by this subtype (Fig. 5D and [28]). This data would suggest that in addition to PDAC patients with squamous subtype, patients whose PDAC display LOH at *KRAS* could also benefit from therapies that aim to inhibit YAP1 activation or activities.

Pancreatic cancer metastasis is believed to be driven by epigenomic reprogramming rather than a genomic mutation signature [20, 21], intriguingly, our data indicates that loss of the WT *KRAS* allele is a significant genomic alteration that can drive tumor progression and metastasis via functional YAP1 activation. Together with the genetic study of Mueller *et al.* [12], our data support a model of pancreatic tumor development in which tumor initiation is driven by a single oncogenic *KRAS* mutation, but progression to invasive/metastatic cancer is promoted by amplification of the mutant *KRAS* allele (incomplete MASI) or loss of the WT *KRAS* allele (complete MASI) (Fig. S1). Our identification of WT KRAS-HIPPO-↓YAP1 signaling axis also has profound implications in KRAS targeting therapies. Specifically, since the suppression of the tumor-suppressive WT KRAS may inadvertently promote tumor metastasis, allele-specific targeting strategies that impair the mutant KRAS-induced oncogenesis but spare the tumor suppressive function of WT KRAS would be obligatory in future therapeutic development. Our data identified YAP1 as an attractive drug target that would not interfere the tumor-suppressive properties of WT KRAS for future therapeutic strategies against oncogenic-KRAS driven cancers.

## Materials and Methods

### Cell lines and cell culture procedures

The human pancreatic cancer cell lines AsPC-1, MIA PaCa-2, PANC-1, were purchased from American Type Culture Collection. To generate stable iWT KRAS cell lines, lentiviral doxycycline-inducible wild-type *KRAS4B* vector [47] were transfected into MIA PaCa-2, AsPC-1, and Panc-1 cell lines using TransDux (System Biosciences, CA, United States) and cell clones were selected with 500 ng/ml puromycin for 2-3 weeks. Each clone's genotype and inducible expression were verified through DNA sequencing, PCR, and Western Blot. For all experiments, cells were trypsinized and allowed to adhere overnight before Doxycycline treatment.

For cell motility assay, confluent monolayer cells (cultured in 6 wells plate) were scratched with a sterile pipette tip. The plates were then washed by DPBS twice and incubated with 10%FBS/DMEM medium at 37°C, with or without Dox for 24 or 48 hours. The rate of migration was calculated by ImageJ using MiToBo plugin28. For colony formation assay, 750 cells were plated in 6-well plates and cultured in 10% FBS/DMEM medium for 12 days. The colonies were stained with crystal violet and analyzed using Colony Area plugin of ImageJ. All experiments were performed at least three times with n=3. MTT assay was performed in 6 replicates as previously described [8]. n=3 can detect a 1.5 fold change with a p-value= 0.05, and with a power of 0.8, if the coefficient of variation is < 0.49. n=6 can detect a 1.5 fold change with a p-value= 0.05, and with a power of 0.8, if the coefficient of variation is < 0.84. These conditions pertain for their respective experiments.

For transient transfections of plasmids HOP-FLASH (Addgene plasmid #833467), HIP-FLASH (Addgene plasmid#83466), pFLAG-YAP1 (Addgene plasmid #66853), and pCMV-flag S127A YAP (Addgene plasmid #27370), cell lines were grown to 90% confluence at the time of transfection. Lipofectamine 2000 (Invitrogen, Catalog #: 11668-027) and Opti-MEM® I Reduced Serum Medium (Catalog #: 31985-062) were used per manufacturer's instruction. Exogenous WT/S127A YAP1 expression were confirmed by anti-flag immunoblots. For reporter assay, pRL-SV40 *Renilla* luciferase vector (Promega, Catalog #: E2231) was co-transfected with HOP-FLASH/HIP-FLASH into cells in 96-well plates in 6 replicates in three independent experiments, and their activities were measured using Dual-Glo Luciferase Assay System (Promega, Catalog #: E2920) on Modulus™ II Microplate Multimode Reader (Promega, Model #: 9310-011) the day after the transfection. The optimized ratio of *Firefly* reporter to *Renilla* reporter vector was 10:1.

For apoptosis assay, propidium iodide (PI, BD Biosciences, Material #: 556463) and Annexin V (BD Biosciences, Material #: 550474) double labeled cells were detected using the BD FACSCantoII. All procedures were performed following the protocol of BD Biosciences Annexin V staining of adherent cells for flow cytometry.

### Immunofluorescence and immunocytochemistry

For immunofluorescence, cells were seeded with or without 2 ug/mL Dox treatment for 24 hours in a 6-well plate with laminin-coated coverslips, harvested at 50%-70% confluence and fixed with 4% paraformaldehyde (PH7.4, Santa Cruz Biotechnology, Inc. Dallas, TX,

United States) in PBS for 10 min at room temperature, washed three times for 5 minutes each by PBS, followed by permeabilization with 0.1% Triton X-100 (Acros Organics, New Jersey, United States) in PBS for 10 min at RT. After blocking with 3% nonfat dry milk in PBS for 1 h, cells were incubated with YAP1 antibody (Novus Biologicals, Catalog #: H00010413-M01, 1:500 dilution) in PBS at RT for 1 hour or at 4°C overnight. After washing with PBS, cells were incubated with Fluorescein (FITC) –conjugated AffiniPure Fab Fragment secondary antibody (Jackson ImmunoResearch Laboratories, Inc. Code #: 111-097-003, 1:200 dilution) at RT for 1 hour. Cell nuclei were counterstained with DAPI (4', 6-Diamidino-2-Phenylindole, Dilactate. Invitrogen, Catalog #: D3571, 1:100 dilute the stock solution) at RT for 3 minutes. Slides were mounted using CITIFOUR Antifadent Mounting Medium (Catalog #: AF87).

Immunofluorescence staining images were collected at room temperature using a 60x/1.49 Apo TIRF oil lens on a Nikon Ti Eclipse inverted microscope. Images were normalized and analyzed by ImageJ. For immunocytochemistry, cells were grown on coverslips and harvested at 50%-70% confluence as described above. All other procedures were performed the same as described for IHC according to the manufacturer's instructions. Immunocytochemistry staining of YAP1 were reviewed by two independent researchers who were blinded to the experimental designs. Ten randomly selected fields of view under 20x objective lens were captured for each slide to calculate the ratio of YAP1 cytoplasmic retention rate (# of cytoplasmic retention cells in the field/ total # of cells in the field).

TMA were constructed from 92 cases of surgical resected PDAC tumor tissues (2013-2014) from the Pancreas Center & Department of General Surgery, The First Affiliated Hospital of Nanjing Medical University, China as previously reported[48] (Table S1). All protocols were reviewed and approved by the Academic Ethics Committee of the First Affiliated Hospital of Nanjing Medical University, China. Informed consents were signed and obtained from all subjects. For IHC, TMA sections derived from the formalin-fixed and paraffin-embedded blocks were deparaffinized and hydrated by routine procedures. Sodium citrate buffer (pH 6.0) was used as the antigen retrieval (100°C, 20 minutes). The primary antibodies at diluted concentrations were incubated overnight at room temperature. Envision+system-HRP (anti-rabbit polymer-HRP, Dako, Code #: K4011) were used as the secondary antibody. The TMA sections were developed with Dako DAB+ Chromogen and Dako Substrate Buffer and then subsequently counterstained with Harris Modified Hematoxylin (Fisher Chemical, Catalog #: SH30-500D) and Scott's Bluing Reagent (RICCA, Catalog #: 6697-1). After drying, sections were mounted with permanent mounting medium (VectaMount, Catalog #: H-5000). TMA slides were sent for scanning by Leica SCN 400 system and analyzed by Aperio ImageScore (Aperio Technologies, Inc.). The quantitation of immunostaining for YAP1 on TMA slides was completed by a pathologist who was blinded to patients' details. The immunostaining score of YAP1 in tumor parenchyma dots was semiquantified by an H-Score based on nuclear staining intensity and the percentage of positive cells (0-100%). Staining intensity was presented as 0, 1, 2, 3 points. Final score equals intensity points multiplied by positive rate percentages. IHC results were divided into three groups according to their final H-score value: Negative (n=32, H-score ≤ 0.1), Low (n=27, 0.1<H-score ≤ 0.6), and High (n=33, 0.6<H-score) (Table S1).

## DNA and RNA analyses

Single-stranded cDNA was synthesized from 2μg of total RNA extracted by Invitrogen SuperScript™ First-Strand Synthesis System (Catalog #: 12371-019) and Qiagen RNeasyPlus Mini Kit (Catalog #: 74104) using Invitrogen SuperScript III Reverse transcriptase kit (REF #: 18080-044). Sequencing was performed by GENEWIZ (South Plainfield, NJ, USA).

For RNA-Seq, RNA samples (n=3) were collected from Dox-treated (2μg/mL) or vehicle-treated iWT-KRAS-MIA PaCa-2 cells in triplicates 48 hours after treatment initiation. Extraction was performed with Qiagen's miRNeasy micro kit. The quality of purified RNA samples was determined using a Bioanalyzer 2100 (Agilent). Samples were only processed if their RIN>8.0. PolyAAA pulldown, amplification, and labeling were performed with the TruSeq mRNA kit. RNA expression was measured on an Illumina HiSeq2000 at the Columbia Genome Center. 30M SE 100 BP reads per sample were taken. RTA (Illumina) was used for base calling and CASAVA (version 1.8.2) [49]for converting BCL to fastq format, and for adaptor trimming.

Reads were mapped to the Grch38 assembly of the human genome with Rsubread [50] and the number of reads per gene were counted with featureCounts [50]. Differential expression was determined with weighted Limma-Voom [51, 52]. Lack of normality is compensated by estimating the variance as a function of mean [51]. A Benjamini-Hochberg false discovery rate, fdr ≤ 0.05 was used as a significance cutoff [53]. n=3 is sufficient to observe a fold-change of 2 with a p-value ≤ 0.001, and a power of 0.80, if the coefficient of variation ≤ 0.2, a value for many genes in this experiment [54]. The use of a p-value ≤ 0.001 is to compensate for multiple testing [55]. The heatmap was generated for 159 genes combined from the “KEGG HIPPO Signaling” and “KEGG HIPPO Signaling Multiple Species” pathways [56]. The volcano plots of YAP1 signature genes was generated with the R graphics package [57].The heatmap was generated with Cluster 3.0 [58, 59] and JavaTreeview [58, 60]. Counts were normalized by the TMM method[61], 1 was added to each count, and then the counts were $\log_2$ transformed. Only HIPPO pathway genes with range($\log_2$ counts)≥1 were included. Genes were mean centered. Uncentered Pearson correlation and average linkage clustering [62] of both genes and samples were used.

Differentially expressed genes were also compared to the Biological Process branch of the Gene Ontology [63] database using the elim method [64], as implemented in iPathwayGuide [65]. The -log10P values of statistically significant (P≤ 0.05) and biologically relevant select Gene Ontology terms were plotted with the barplot command in the R stats package [57].

Real-time quantitative PCR was performed using the ABI Prism 7500 Sequence Detector and Mx3000P QPCR System with the Applied Biosystems Power SyBr Green PCR Master Mix (REF #: 4367659). All reactions were performed in triplicate. The transcriptional expression level of each target gene was normalized to Homo glyceraldehyde-3-phosphate dehydrogenase (GAPDH). Relative gene expression was calculated according to the ΔΔCt method. The sequences of the primers used in the study are listed in Table S2.

To determine human PDAC samples with or without LOH at *KRAS*, we used the TCGA mutation data to collect potential *KRAS* mutations in PDAC, samtools to extract *KRAS* counts from BAM files, counted *KRAS* mutation at the TCGA reported hotspots, calculated mutation vs. reference percentage to infer *KRAS* LOH status. Hierarchical clustering analysis of human PDAC samples with the YAP1 activation signature and the association of YAP1 signature score and the LOH at *KRAS* status were performed as previously described [28].

## Western Blot and Co-IP

Cells were harvested at 90% confluence with or without 2 μg/mL doxycycline treatment for 24 hours or as otherwise indicated. For western blots, cell lysates were prepared using RIPA Lysis Buffer (Millipore, Catalog#: 20-188). Separation of nuclear and cytoplasmic protein extraction was done using the NE-PER Nuclear and Cytoplasmic Extraction Reagents (Catalog #: 78833). For Co-IP, cells were lysed in NETN lysis buffer (20 mM Tris–HCl pH 8.0, 100 mM NaCl, 0.5% NP-40, 1 mM EDTA). 1μg of antibody was added to the cleared lysate and incubated overnight. Then, 20μl of protein A/G agarose was added to the lysate, incubated for 4 hours, then washed with NETN three times. Protease inhibitor tablet (Pierce, Prod#: 88266) and Halt™ phosphatase inhibitor cocktail (Prod #: 1862495) were added into the Lysis Buffer before scratching the cells. Concentration of cell lysates were determined using the Pierce™ BCA Protein Assay Kit (Catalog #: 23225/23227). Proteins were separated using NuPAGE™ 10% Bis-Tris Gel (REF #: NP0301BOX). Protein transfer was performed by using the XCell II™ Blot Module (Invitrogen, Catalog #: EI9051). After the transfer, membranes were blocked with 3-5% non-fat milk at room temperature for one hour and incubated with primary antibody at 4 degree overnight, secondary antibody at room temperature for one hour. The HRP reaction was performed with SuperSignal® Chemiluminescent Substrate (Catalog #: 34080) and then imaging was performed by Odyssey® Fc Imaging System. Details regarding antibody usage are available in Table S3. Western blot and Co-PI analyses were quantified using Image J; GAPDH, β-actin, or Lamin B1 (nuclear proteomic analysis) expression was used to normalize potential sample loading differences. Results were plotted as mean±standard deviation (SD) of three independent experiments.

## Proteomic analyses

**Sample preparation—**$5x10^6$ frozen cell pellets from each condition (n=5) were used to perform subcellular protein fractionation. Minute Cytoplasmic and Nuclear Extraction kit (Invent Biotech, MN) was used to prepare nuclear and cytoplasmic fractions according to the manufacturer's instruction. Protein concentration was measured by Qubit Protein Quantification Assay (Thermo Fisher, Rockford, IL). 35μg of protein lysate (nuclear or cytoplasmic) from each sample were trapped and digested by trypsin on a micro S-trap column (PROTIFI, NY) according to the manufacturer's instruction. 0.6μg of the peptide mixture was used for peptide quantification assay (Thermo Fisher, Rockford, IL).

Isobaric labeling of peptides was performed using the 11-plex tandem mass tag (TMT) reagents (Thermo Fisher Scientific, Rockford, IL). TMT reagents (0.8mg) were dissolved in 41μl of dry acetonitrile (ACN), and 20.5μl was added to 25μg of digested peptide in 100mM

TEAB. After 1 hour incubation at room temperature, the reaction was quenched by adding 4.2μl of 5% hydroxylamine. Labeled peptides were combined and dried for the subsequent high pH reverse phase peptide fractionation (Thermo Fisher, Rockford, IL). 8 fractions were generated for each combined set. Each TMT labeled fraction was reconstituted in a solution of 2 % acetonitrile (ACN), 2 % formic acid (FA) for MS analysis.

**LC-MS/MS analysis—**1/10 (by volume) of peptides from each fraction were loaded and analyzed using an EasySpray column (Thermo Fisher, ES903) and a Dionex UltiMate 3000 UHPLC. See Supplementary Method for gradient setting and time. Peptides were electrosprayed and analyzed using the Thermo Fusion Tribrid mass spectrometer equipped with an EASY-Spray source (Thermo Finnigan, San Jose, CA). See Supplementary Method for mass spectrometer setting.

**Data analysis—**Tandem mass spectra from raw files were searched against a human protein database using the Proteome Discoverer 2.1 (Thermo Finnigan, San Jose, CA). The Proteome Discoverer application extracts relevant MS/MS spectra from the .raw file and determines the precursor charge state and the quality of the fragmentation spectrum. The Proteome Discoverer probability-based scoring system rates the relevance of the best matches found by the SEQUEST algorithm. The human protein database was downloaded as FASTA-formatted sequences from UniProt protein database (released in January, 2017). The peptide mass search tolerance was set to 10ppm. A minimum sequence length of 7 amino acids residues was required. Only fully tryptic peptides were considered. To calculate confidence levels and false positive rates (FDR), Proteome Discoverer generates a decoy database containing reverse sequences of the non-decoy protein database and performs the search against this concatenated database (non-decoy + decoy). 1% FDR was used to generate the quantitative list for statistical analysis. For quantification, a 0.003 m/z (10plex TMT) window centered on the theoretical m/z value of each reporter ion was queried for the nearest signal intensity. Reporter ion intensities were adjusted for the isotopic impurities of each TMT reagent according to the manufacture specifications. The signal-to-noise (S/N) values for all peptides were summed within each TMT channel, and each channel was scaled according to the inter-channel difference of these sums to account for differences in sample handling. For each peptide, a total minimum sum S/N of 10 and an isolation purity greater than 75% was required. Total peptide amount was used for normalization to correct for experimental bias.

**Statistical analysis—**Using the Qlucore Omics Explorer 2.2, ANOVA was applied to generate a protein signature from each comparison. Multiple test correction was performed by adjusting the calculated p-values according to Benjamini-Hochberg. False discovery rate was reported for each comparison. Statistical analysis was performed by using GraphPad Prism (version 6.01; GraphPad Software, Inc., La Jolla, CA) and Qlucore Omics Explorer (Qlucore AB, Lund, Sweden). To identify protein signatures which distinguish among groups, we applied ANOVA to the dataset using the Qlucore Omics Explorer. The k-nearest neighbor method (kNN) was used to impute missing values for proteomic analysis. Log transformed values were used for statistical analysis, to approximate normality, and different experimental batch effect was controlled in all statistical analysis by adjusting batch

variables or normalizing data with endogenous protein values. n=5 is sufficient to observe a fold-change of 2 with a p-value ≤ 0.001, and a power of 0.80, if the coefficient of variation ≤ 0.25, a value for many proteins in this experiment [54]. The use of a p-value ≤ 0.001 is to compensate for multiple testing [55].

### Xenograft model

Approximately 1 million cells in log phase growth were subcutaneously injected into each flank (bilateral) of the nude mice (Female Crl: NU-Foxn1nu, 5-6 weeks old from Charles River, Wilmington, MA, USA). 3 mice per group, with 2 implantations per animal were used. The mice were provided with drinking water containing Dox 2mg/ml or vehicle control for two weeks and the size of the tumors were monitored and recorded every other day. Treatments were initiated at the time of implantation, so no randomization was employed. The tumor sizes were recorded by one investigator and the data were analyzed by two investigators (not blinded). The experiments were repeated for confirmation. n=3 is sufficient to observe a 1.5 fold change in tumor size with a p-value ≤ 0.05, and a power of 0.8, if the coefficient of variation is ≤ 0.49, a condition that pertains in the present experiment. All mice were housed in the Animal Care Facility at Columbia University Irving Medical Center (CUIMC), and the studies were conducted in compliance with the CUIMC Institutional Animal Care and Use Committee (IACUC) guidelines.

### Statistical analyses

qqplots and the Shapiro-wilk test were used to test for normality. The statistical significance for each study was determined by two tailed unequal variance Student's t-test, or in the case of multiple conditions, ANOVA unless otherwise specified.

## Data and materials availability:

RNASeq data has been deposited in the Gene Expression Omnibus (GEO) with Accession GSE156562. Proteomics data have been uploaded to the MassIVE data repository site with the accession ID: MassIVE MSV000088107.

## Supplementary Material

Refer to Web version on PubMed Central for supplementary material.

## Acknowledgments:

This study was supported by NIH/NCI R01 CA178445, NIH/NCI R01 CA217207, CUIMC Irving Drug Discovery Pilot Award (HICCC_FY21IDD01), and NIH P30CA013696 for the HICCC. Han Yan was supported by the China Scholarship Council for research at the CUIMC. Ye-Ran Yang was supported by the Morgan Stanley Children's Hospital-Beijing Children's Hospital Program. Dillon C. Karg was supported by the NCI-ICBP (Integrative Cancer Biology Program) Summer Research Program.

## References

1. Siegel RL, Miller KD, Jemal A. Cancer statistics, 2019. CA Cancer J Clin 2019; 69: 7–34. [PubMed: 30620402]
2. Von Hoff DD, Ervin T, Arena FP, Chiorean EG, Infante J, Moore M et al. Increased survival in pancreatic cancer with nab-paclitaxel plus gemcitabine. *The New England journal of medicine*

(Clinical Trial, Phase III Multicenter Study Randomized Controlled Trial Research Support, Non-U.S. Gov't) 2013; 369: 1691–1703.

3. Stephen AG, Esposito D, Bagni RK, McCormick F. Dragging ras back in the ring. Cancer Cell 2014; 25: 272–281. [PubMed: 24651010]
4. Cox AD, Fesik SW, Kimmelman AC, Luo J, Der CJ. Drugging the undruggable RAS: Mission possible? Nat Rev Drug Discov 2014; 13: 828–851. [PubMed: 25323927]
5. Rodriguez-Viciana P, Sabatier C, McCormick F. Signaling specificity by Ras family GTPases is determined by the full spectrum of effectors they regulate. Mol Cell Biol 2004; 24: 4943–4954. [PubMed: 15143186]
6. Soh J, Okumura N, Lockwood WW, Yamamoto H, Shigematsu H, Zhang W et al. Oncogene mutations, copy number gains and mutant allele specific imbalance (MASI) frequently occur together in tumor cells. PLoS One (Research Support, N.I.H., Extramural Research Support, Non-U.S. Gov't) 2009; 4: e7464.
7. Yu CC, Qiu W, Juang CS, Mansukhani MM, Halmos B, Su GH. Mutant allele specific imbalance in oncogenes with copy number alterations: Occurrence, mechanisms, and potential clinical implications. Cancer Lett 2017; 384: 86–93. [PubMed: 27725226]
8. Qiu W, Sahin F, Iacobuzio-Donahue CA, Garcia-Carracedo D, Wang WM, Kuo CY et al. Disruption of p16 and activation of Kras in pancreas increase ductal adenocarcinoma formation and metastasis in vivo. *Oncotarget* (Research Support, N.I.H., Extramural Research Support, Non-U.S. Gov't) 2011; 2: 862–873.
9. Krasinskas AM, Moser AJ, Saka B, Adsay NV, Chiosea SI. KRAS mutant allele-specific imbalance is associated with worse prognosis in pancreatic cancer and progression to undifferentiated carcinoma of the pancreas. *Mod Pathol* (Research Support, N.I.H., Extramural Research Support, Non-U.S. Gov't) 2013; 26: 1346–1354.
10. Chiosea SI, Sherer CK, Jelic T, Dacic S. KRAS mutant allele-specific imbalance in lung adenocarcinoma. Mod Pathol 2011; 24: 1571–1577. [PubMed: 21743433]
11. Malapelle U, Sgariglia R, De Stefano A, Bellevicine C, Vigliar E, de Biase D et al. KRAS mutant allele-specific imbalance (MASI) assessment in routine samples of patients with metastatic colorectal cancer. J Clin Pathol 2015; 68: 265–269. [PubMed: 25609577]
12. Mueller S, Engleitner T, Maresch R, Zukowska M, Lange S, Kaltenbacher T et al. Evolutionary routes and KRAS dosage define pancreatic cancer phenotypes. Nature 2018; 554: 62–68. [PubMed: 29364867]
13. Modrek B, Ge L, Pandita A, Lin E, Mohan S, Yue P et al. Oncogenic activating mutations are associated with local copy gain. *Mol Cancer Res* (Research Support, Non-U.S. Gov't) 2009; 7: 1244–1252.
14. Zhou B, Der CJ, Cox AD. The role of wild type RAS isoforms in cancer. Semin Cell Dev Biol 2016; 58: 60–69. [PubMed: 27422332]
15. Zhang Z, Wang Y, Vikis HG, Johnson L, Liu G, Li J et al. Wildtype Kras2 can inhibit lung carcinogenesis in mice. *Nature genetics* (Research Support, U.S. Gov't, P.H.S.) 2001; 29: 25–33.
16. To MD, Wong CE, Karnezis AN, Del Rosario R, Di Lauro R, Balmain A. Kras regulatory elements and exon 4A determine mutation specificity in lung cancer. Nature genetics 2008; 40: 1240–1244. [PubMed: 18758463]
17. To MD, Rosario RD, Westcott PM, Banta KL, Balmain A. Interactions between wild-type and mutant Ras genes in lung and skin carcinogenesis. Oncogene 2013; 32: 4028–4033. [PubMed: 22945650]
18. Ambrogio C, Kohler J, Zhou ZW, Wang H, Paranal R, Li J et al. KRAS Dimerization Impacts MEK Inhibitor Sensitivity and Oncogenic Activity of Mutant KRAS. Cell 2018; 172: 857–868 e815. [PubMed: 29336889]
19. Staffas A, Karlsson C, Persson M, Palmqvist L, Bergo MO. Wild-type KRAS inhibits oncogenic KRAS-induced T-ALL in mice. Leukemia. 2015;29:1032–40. [PubMed: 25371176]
20. Makohon-Moore AP, Zhang M, Reiter JG, Bozic I, Allen B, Kundu D et al. Limited heterogeneity of known driver gene mutations among the metastases of individual patients with pancreatic cancer. Nature genetics 2017; 49: 358–366. [PubMed: 28092682]

21. McDonald OG, Li X, Saunders T, Tryggvadottir R, Mentch SJ, Warmoes MO et al. Epigenomic reprogramming during pancreatic cancer progression links anabolic glucose metabolism to distant metastasis. Nature genetics 2017; 49: 367–376. [PubMed: 28092686]
22. Harvey KF, Zhang X, Thomas DM. The Hippo pathway and human cancer. Nat Rev Cancer 2013; 13: 246–257. [PubMed: 23467301]
23. Zhao B, Tumaneng K, Guan KL. The Hippo pathway in organ size control, tissue regeneration and stem cell self-renewal. Nat Cell Biol 2011; 13: 877–883. [PubMed: 21808241]
24. Cordenonsi M, Zanconato F, Azzolin L, Forcato M, Rosato A, Frasson C et al. The Hippo Transducer TAZ Confers Cancer Stem Cell-Related Traits on Breast Cancer Cells. Cell 2011; 147: 759–772. [PubMed: 22078877]
25. Kim NG, Gumbiner BM. Adhesion to fibronectin regulates Hippo signaling via the FAK-Src-PI3K pathway. J Cell Biol 2015; 210: 503–515. [PubMed: 26216901]
26. Zhao B, Wei X, Li W, Udan RS, Yang Q, Kim J et al. Inactivation of YAP oncoprotein by the Hippo pathway is involved in cell contact inhibition and tissue growth control. Genes Dev 2007; 21: 2747–2761. [PubMed: 17974916]
27. Gibson-Corley KN, Olivier AK, Meyerholz DK. Principles for valid histopathologic scoring in research. Vet Pathol 2013; 50: 1007–1015. [PubMed: 23558974]
28. Tu B, Yao J, Ferri-Borgogno S, Zhao J, Chen S, Wang Q, et al. YAP1 oncogene is a context-specific driver for pancreatic ductal adenocarcinoma. JCI Insight. 2019;4: e130811. 10.1172/jci.insight.13081.
29. Aguirre AJ, Hruban RH, Raphael BJ, Network CGAR. Integrated Genomic Characterization of Pancreatic Ductal Adenocarcinoma. Cancer Cell 2017; 32: 185-+. [PubMed: 28810144]
30. Singh A, Sowjanya AP, Ramakrishna G. The wild-type Ras: road ahead. *FASEB J* (Research Support, N.I.H., Extramural Research Support, U.S. Gov't, P.H.S. Review) 2005; 19: 161–169.
31. Matallanas D, Romano D, Al-Mulla F, O'Neill E, Al-Ali W, Crespo P et al. Mutant K-Ras activation of the proapoptotic MST2 pathway is antagonized by wild-type K-Ras. *Mol Cell* (Research Support, Non-U.S. Gov't) 2011; 44: 893–906.
32. Romano D, Maccario H, Doherty C, Quinn NP, Kolch W, Matallanas D. The differential effects of wild-type and mutated K-Ras on MST2 signaling are determined by K-Ras activation kinetics. *Mol Cell Biol* (Research Support, Non-U.S. Gov't) 2013; 33: 1859–1868.
33. Young A, Lou D, McCormick F. Oncogenic and wild-type Ras play divergent roles in the regulation of mitogen-activated protein kinase signaling. *Cancer Discovery* (Research Support, Non-U.S. Gov't) 2013; 3: 112–123.
34. Grabocka E, Pylayeva-Gupta Y, Jones MJ, Lubkov V, Yemanaberhan E, Taylor L et al. Wild-type H- and N-Ras promote mutant K-Ras-driven tumorigenesis by modulating the DNA damage response. *Cancer Cell*(Research Support, N.I.H., Extramural) 2014; 25: 243–256.
35. Vartanian S, Bentley C, Brauer MJ, Li L, Shirasawa S, Sasazuki T et al. Identification of mutant K-Ras-dependent phenotypes using a panel of isogenic cell lines. J Biol Chem 2013; 288: 2403–2413. [PubMed: 23188824]
36. Overholtzer M, Zhang J, Smolen GA, Muir B, Li W, Sgroi DC et al. Transforming properties of YAP, a candidate oncogene on the chromosome 11q22 amplicon. Proc Natl Acad Sci U S A 2006; 103: 12405–12410. [PubMed: 16894141]
37. Sun T, Chi JT. Regulation of ferroptosis in cancer cells by YAP/TAZ and Hippo pathways: The therapeutic implications. Genes Dis 2021; 8: 241–249. [PubMed: 33997171]
38. Moroishi T, Hansen CG, Guan KL. The emerging roles of YAP and TAZ in cancer. *Nature Reviews Cancer* (Research Support, N.I.H., Extramural Research Support, Non-U.S. Gov't Review) 2015; 15: 73–79.
39. Shao DD, Xue W, Krall EB, Bhutkar A, Piccioni F, Wang X et al. KRAS and YAP1 converge to regulate EMT and tumor survival. Cell 2014; 158: 171–184. [PubMed: 24954536]
40. Hong X, Nguyen HT, Chen Q, Zhang R, Hagman Z, Voorhoeve PM et al. Opposing activities of the Ras and Hippo pathways converge on regulation of YAP protein turnover. EMBO J 2014; 33: 2447–2457. [PubMed: 25180228]

41. Zhang W, Nandakumar N, Shi Y, Manzano M, Smith A, Graham G et al. Downstream of mutant KRAS, the transcription regulator YAP is essential for neoplastic progression to pancreatic ductal adenocarcinoma. Sci Signal 2014; 7: ra42. [PubMed: 24803537]
42. Kapoor A, Yao W, Ying H, Hua S, Liewen A, Wang Q et al. Yap1 activation enables bypass of oncogenic Kras addiction in pancreatic cancer. Cell 2014; 158: 185–197. [PubMed: 24954535]
43. Salcedo Allende MT, Zeron-Medina J, Hernandez J, Macarulla T, Balsells J, Merino X et al. Overexpression of Yes Associated Protein 1, an Independent Prognostic Marker in Patients With Pancreatic Ductal Adenocarcinoma, Correlated With Liver Metastasis and Poor Prognosis. Pancreas 2017; 46: 913–920. [PubMed: 28697132]
44. Gruber R, Panayiotou R, Nye E, Spencer-Dene B, Stamp G, Behrens A. YAP1 and TAZ Control Pancreatic Cancer Initiation in Mice by Direct Up-regulation of JAK-STAT3 Signaling. Gastroenterology 2016; 151: 526–539. [PubMed: 27215660]
45. Volodko N, Gordon M, Salla M, Ghazaleh HA, Baksh S. RASSF tumor suppressor gene family: biological functions and regulation. FEBS Lett 2014; 588: 2671–2684. [PubMed: 24607545]
46. Avruch J, Xavier R, Bardeesy N, Zhang XF, Praskova M, Zhou D et al. Rassf family of tumor suppressor polypeptides. J Biol Chem 2009; 284: 11001–11005. [PubMed: 19091744]
47. Lampson BL, Pershing NL, Prinz JA, Lacsina JR, Marzluff WF, Nicchitta CV et al. Rare codons regulate KRas oncogenesis. *Curr Biol* (Research Support, N.I.H., Extramural Research Support, Non-U.S. Gov't) 2013; 23: 70–75.
48. Yan H, Qiu W, Koehne de Gonzalez AK, Wei JS, Tu M, Xi CH et al. HHLA2 is a novel immune checkpoint protein in pancreatic ductal adenocarcinoma and predicts post-surgical survival. Cancer Lett 2019; 442: 333–340. [PubMed: 30447255]
49. Hosseini P, Tremblay A, Matthews BF, Alkharouf NW. An efficient annotation and gene-expression derivation tool for Illumina Solexa datasets. BMC Res Notes 2010; 3: 183. [PubMed: 20598141]
50. Liao Y, Smyth GK, Shi W. featureCounts: an efficient general purpose program for assigning sequence reads to genomic features. Bioinformatics 2014; 30: 923–930. [PubMed: 24227677]
51. Law CW, Chen Y, Shi W, Smyth GK. voom: Precision weights unlock linear model analysis tools for RNA-seq read counts. Genome Biol 2014; 15: R29. [PubMed: 24485249]
52. Liu R, Holik AZ, Su S, Jansz N, Chen K, Leong HS et al. Why weight? Modelling sample and observational level variability improves power in RNA-seq analyses. Nucleic Acids Res 2015.
53. Benjamini Y, Hochberg Y. Controlling the false discovery rate; A practical and powerful approach to multiple testing. J Roy Stat Soc Ser B 1995; 57: 289–300.
54. Hart SN, Therneau TM, Zhang YJ, Poland GA, Kocher JP. Calculating Sample Size Estimates for RNA Sequencing Data. J Comput Biol 2013; 20: 970–978. [PubMed: 23961961]
55. Simon R, Radmacher MD, Dobbin K. Design of studies using DNA microarrays. Genet Epidemiol 2002; 23: 21–36. [PubMed: 12112246]
56. Kanehisa M, Goto S, Kawashima S, Okuno Y, Hattori M. The KEGG resource for deciphering the genome. Nucleic Acids Res 2004; 32: D277–280. [PubMed: 14681412]
57. R Core Team. R: A Language and Environment for Statistical Computing}, 4.0.0 edn. R Foundation for Statistical Computing: Vienna, Austria, 2020.
58. Eisen MB, Spellman PT, Brown PO, Botstein D. Cluster analysis and display of genome-wide expression patterns. Proc Natl Acad Sci USA 1998; 95: 14863–14868. [PubMed: 9843981]
59. de Hoon MJ, Imoto S, Nolan J, Miyano S. Open source clustering software. Bioinformatics 2004; 20: 1453–1454. [PubMed: 14871861]
60. Saldanha AJ. Java Treeview--extensible visualization of microarray data. Bioinformatics 2004; 20: 3246–3248. [PubMed: 15180930]
61. Robinson MD, Oshlack A. A scaling normalization method for differential expression analysis of RNA-seq data. Genome Biol 2010; 11: R25. [PubMed: 20196867]
62. Everitt BS, Landau S, Leese M, Stahl D. Cluster analysis. Wiley, 5th edition. John Wiley & Sons., Inc. 2011. https://onlinelibrary.wiley.com/doi/book/10.1002/9780470977811.

63. Ashburner M, Ball CA, Blake JA, Botstein D, Butler H, Cherry JM, et al. Gene ontology: tool for the unification of biology. The Gene Ontology Consortium. Nat Genet. 2000;25:25–9. 10.1038/75556. [PubMed: 10802651]

64. Alexa A, Rahnenfuhrer J, Lengauer T. Improved scoring of functional groups from gene expression data by decorrelating GO graph structure. *Bioinformatics* (Research Support, Non-U.S. Gov't) 2006; 22: 1600–1607.

65. Ahsan S, Draghici S. Identifying Significantly Impacted Pathways and Putative Mechanisms with iPathwayGuide. Curr Protoc Bioinformatics 2017; 57: 7 15 11–17 15 30. [PubMed: 28654712]

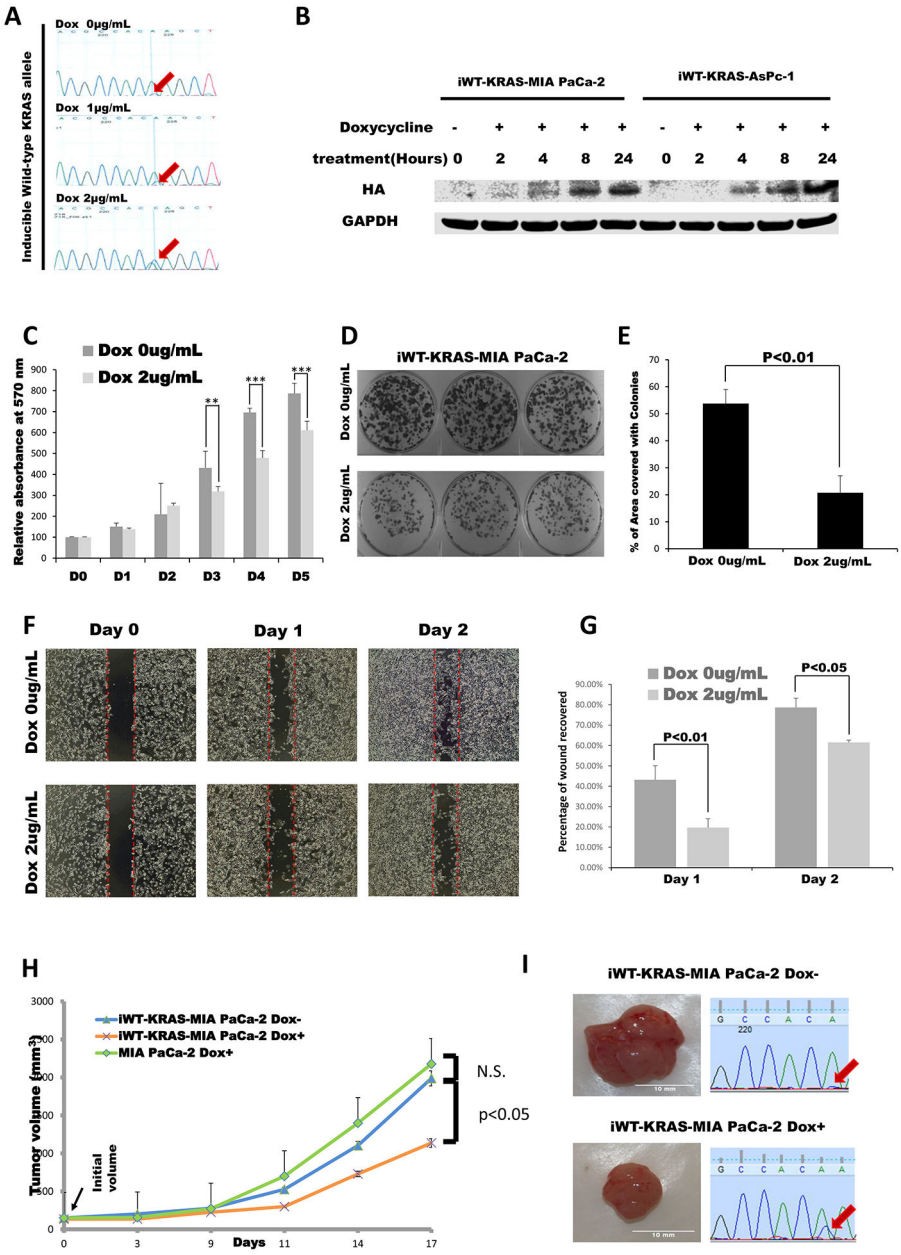


**Figure 1. Restored wild-type KRAS expression in pancreatic cancer cell lines attenuated tumor malignancies *in vitro* and *in vivo*.**

**A.** Sanger sequencing of cDNA showed a Dox dosage-dependent induction of the wild-type *KRAS* (the wild-type allele is marked by arrows) in the iWT-KRAS-MIA PaCa-2 cells. **B**. Time-dependent wild-type KRAS protein expression at 2μg/ml Dox treatment as demonstrated by western blot analysis. Exogenous wild-type KRAS protein expression could be differentiated from endogenous KRAS with the HA tag. Inhibitory effects of the induced wild-type KRAS expression on the iWT-KRAS-MIA PaCa-2 cells were demonstrated by the MTT (**C**), colony formation (**D-E**), and cell motility assays (**F-G**). **H-I.** Re-expression of the wild-type *KRAS* allele in the iWT-KRAS-MIA PaCa-2 cells reduced

tumor growth in subcutaneous xenograft models. The induced expression of the wild-type *KRAS* (arrow) in the tumors was confirmed by Sanger sequencing of cDNA.

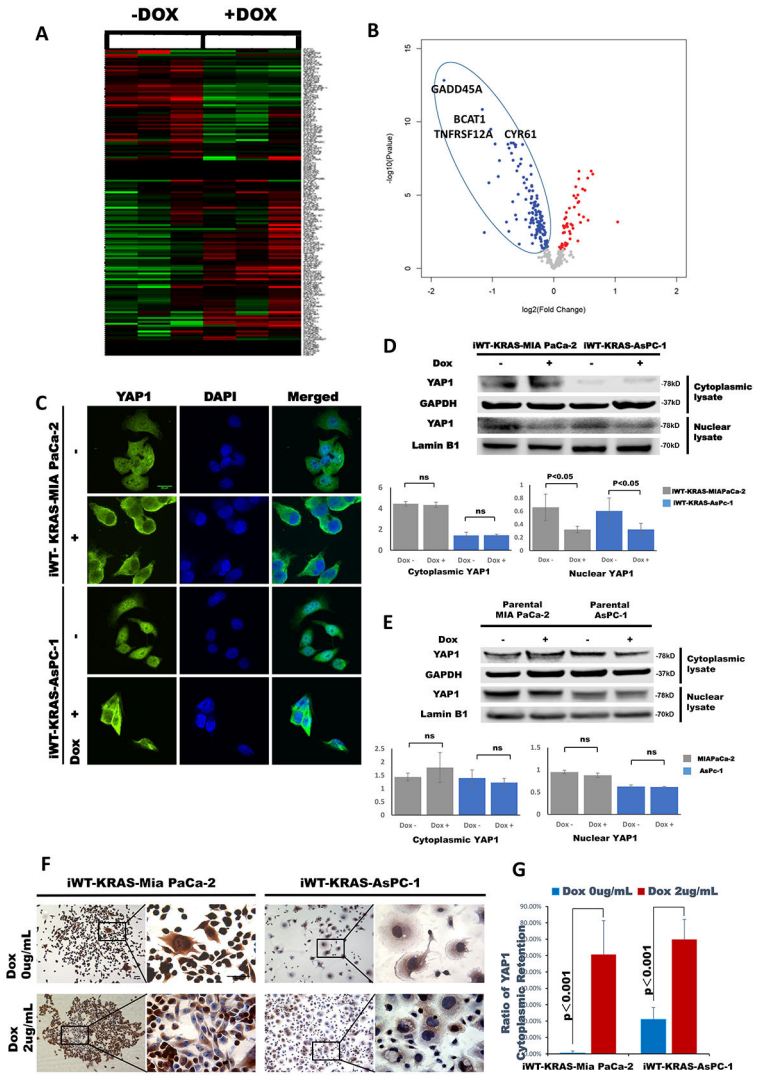


**Figure 2. Induced WT KRAS expression attenuated YAP1 activation in the iWT KRAS MIA PaCa-2 and iWT KRAS AsPC-1 cell lines.**

**A.** RNA-Seq analyses comparing Dox-treated *vs.* vehicle-treated iWT-KRAS-MIA PaCa-2 cells revealed that genes in the HIPPO pathway were differentially expressed with WT *KRAS* expression, fdr ≤ 0.05. **B.** Volcano plots of the YAP1 target genes from the same RNA-Seq dataset with p<0.05 significance cutoff and log2FC>0.585. Nuclear YAP1 localization was inhibited in the Dox-treated iWT KRAS cells but not in the vehicle-treated iWT KRAS control or Dox-treated parental cell lines at 24 hour-timepoint **(C-G). C**. Representative images of immunofluorescence labeling of YAP1 subcellular localization (green) in the iWT KRAS cell lines. Nuclei were counterstained with DAPI. Scale bar equals to 20μm. **D-E**. Nuclear and cytoplasmic lysates of the iWT KRAS or parental cell lines were extracted and analyzed by western blot analysis. Quantifications are presented in mean±SD of three independent experiments. **F-G** Quantitative analysis of YAP1 immunocytochemistry (mean±SD). Bar, 50μm. *p*-values are shown in the charts; ns= not significant.

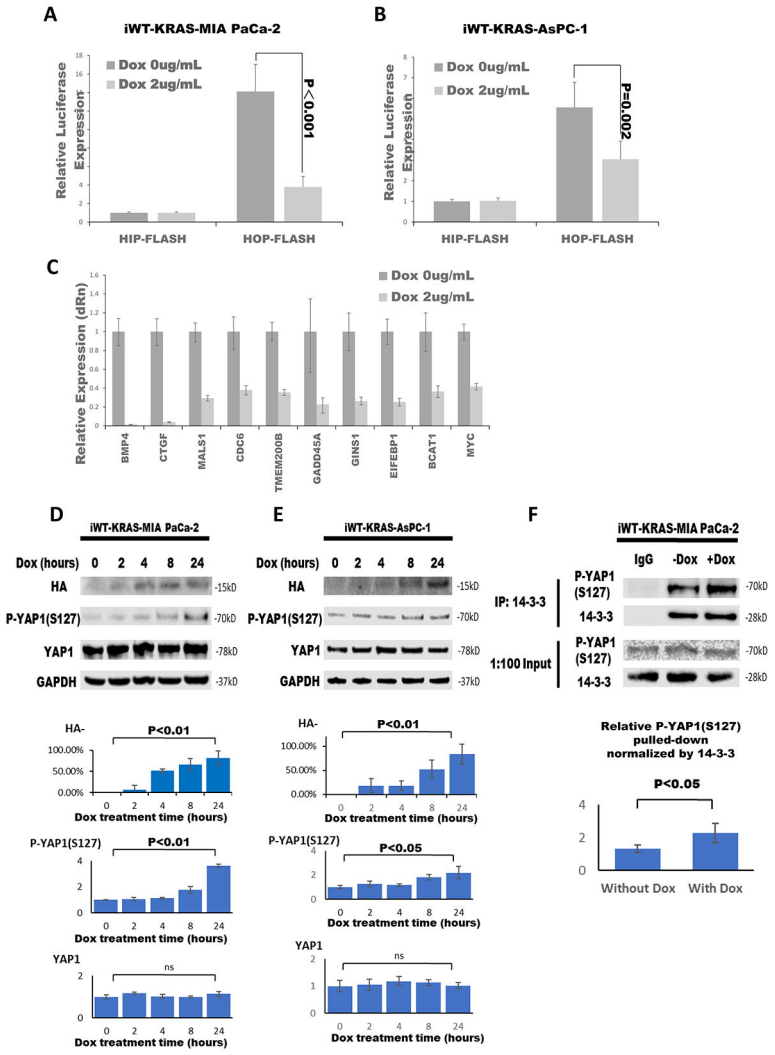


**Figure 3. The restoration of WT KRAS expression led to enhanced YAP1-14-3-3zeta binding and reduced YAP1-TEAD activities.**

**A-B.** iWT-KRAS cell lines were transiently co-transfected with HIP-flash/HOP-flash reporters and pRL-SV40 *Renilla* reporter (control). Dox-induced WT KRAS expression suppressed the activity of YAP1-specific HOP-FLASH reporter. **C.** Selected YAP-TEAD target genes were verified by qRT-PCR. **D-E.** Western Blot analyses showing an elevated level of phosphorylated-YAP1(S127) in the iWT-KRAS cells correlated with increasing WT KRAS expression (HA-tag) post Dox treatment. Quantifications are presented in mean±SD of three independent experiments. The statistical analyses were performed between timepoint 0 and 24 hours of the Doxycycline treatment. **F.** Co-IP analysis with anti-14-3-3 antibody showed an enhanced interaction of p-YAP1(S127) with endogenous 14-3-3 upon the restoration of WT KRAS. *p*-values are shown in the charts; ns= not significant.

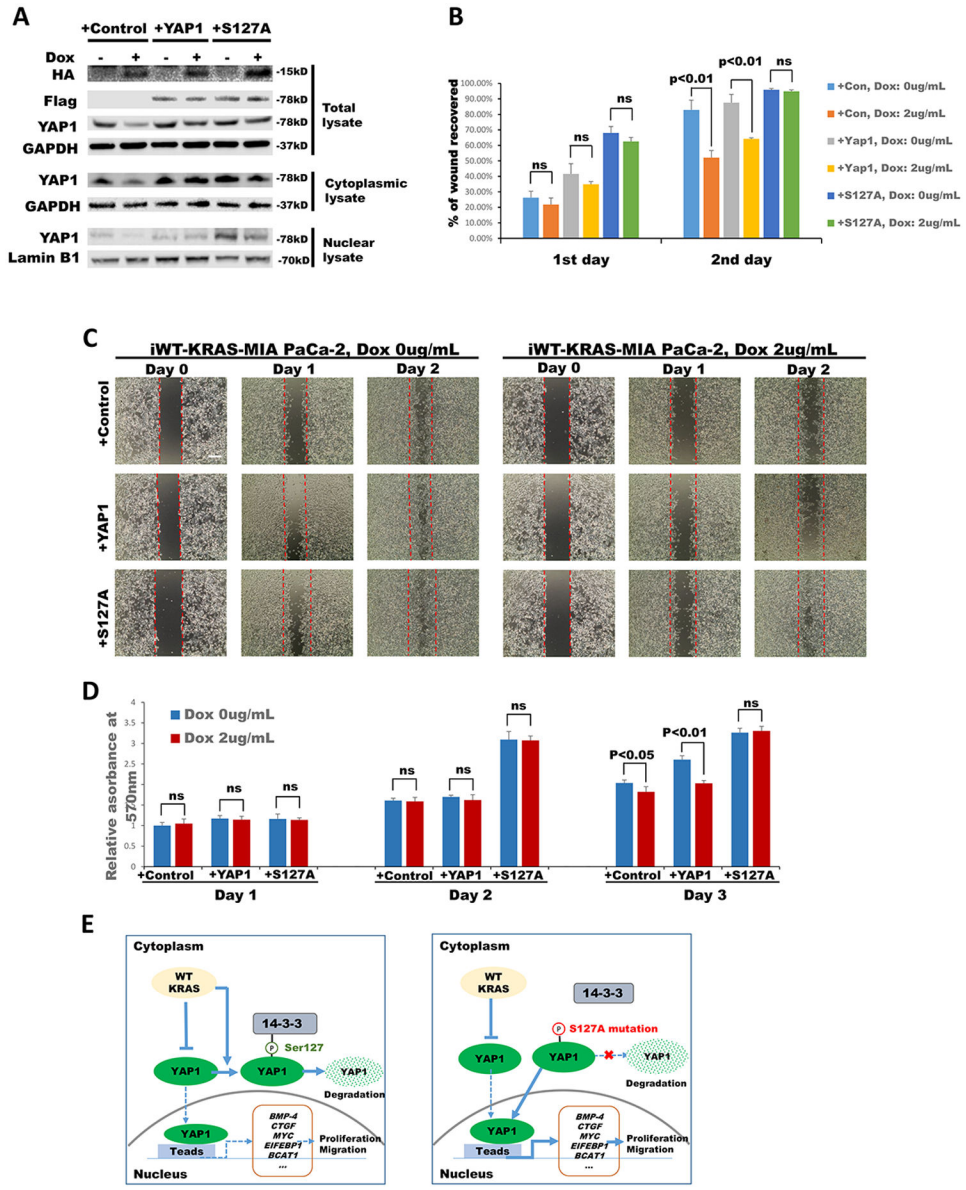


**Figure 4. The S127A mutant YAP1 reversed the tumor-suppression exerted by the wild-type *KRAS* allele in the iWT-KRAS-Mia PaCa-2 cells.**

**A**. iWT-KRAS-MIA PaCa-2 cells were transiently transfected with the S127A mutant YAP1 plasmid. The empty vector and the wild-type YAP1 plasmid served as the negative and positive control, respectively. Transfected cells were treated with 2 ug/mL Dox or vehicle control for 24 hours, followed by western analyses. **B-C**. Motility assay showed that the introduction of the S127A mutant YAP1, but not the wild-type YAP1, into the iWT-KRAS cells could overcome the WT KRAS-induced suppression. Scale bar, 100μm. **D**. MTT assays demonstrated that the S127A mutant YAP1 expression in the iWT-KRAS-MIA PaCa-2 cells rescued the cells from the WT KRAS-induced growth suppression. **E**. Diagram depicts our working model that WT KRAS exerts its tumor suppression by enhancing 14-3-3 interaction with YAP1 at S127 and retaining YAP1 proteins in the cytoplasm. This working model is supported by the facts that S127A mutant YAP1, which can no longer be bound by 14-3-3,

could bypass wild-type KRAS-induced tumor suppression. *p*-values are shown in the charts; ns= not significant.

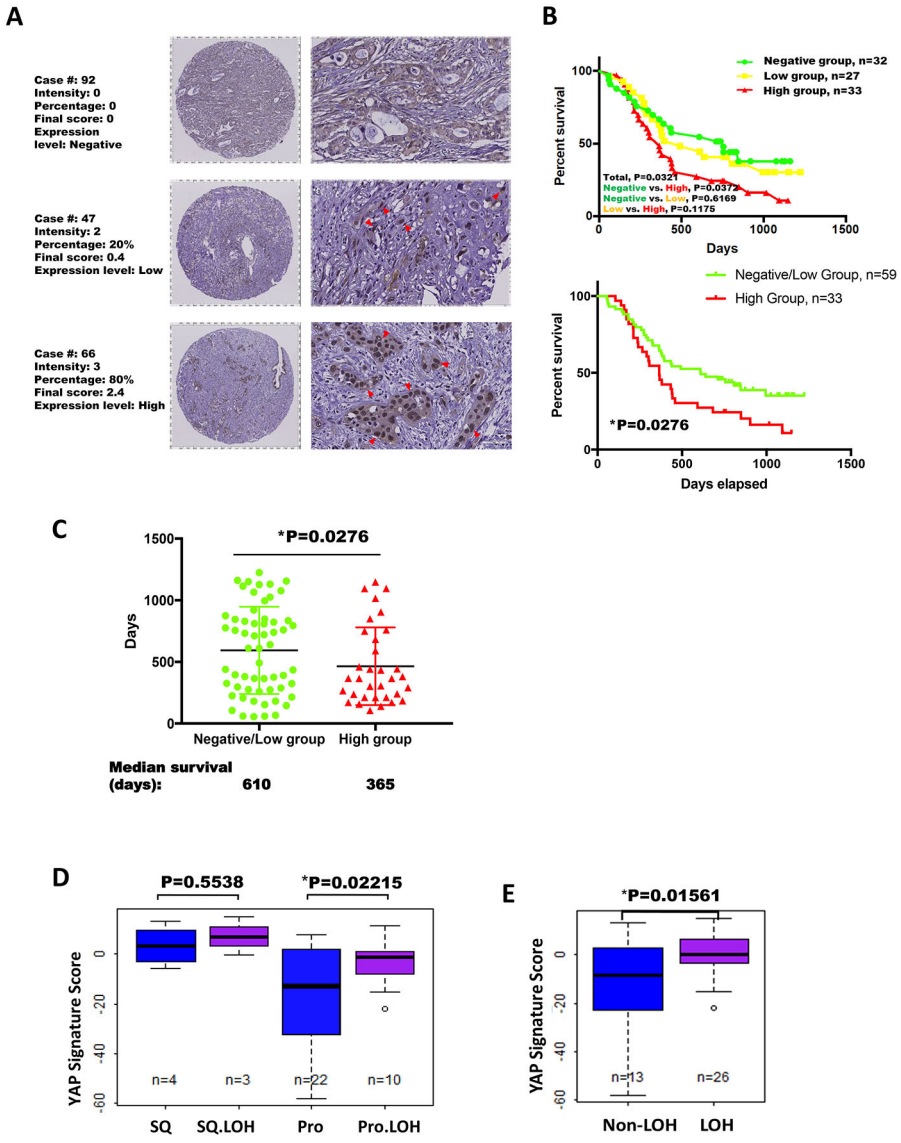


**Figure 5. LOH at *KRAS* was positively associated with the increased expression of the YAP1 activation signature in human PDAC samples.**

**A-C**. Nuclear YAP1 expression was negatively associated with post-surgical survival of PDAC patients as quantified by H-score. **A.** Representatives of each group are shown here, with areas with substantial positive labeling highlighted by arrows. **B.** Kaplan-Meier analyses of the prognostic significances of activated YAP1 in these patients. PDAC patients with high nuclear YAP1 expressions had statistically significant shorter survival than those the negative or negative/low groups. **C**. Median survival (days) of each group was shown by scatter plot with 95% CI. **D.** YAP1 signature scores among human PDAC basal and progenitor subtypes, with or without LOH at *KRAS*. **E.** Without subtype distinction, YAP1 signature score was statistically elevated in human PDAC samples with LOH at *KRAS* compared to those without LOH at *KRAS*.